Supporting Information

Revisiting the Interfacial Chemistry of Calcium Metal Anodes: The Importance of Inorganic-Rich Solid/Electrolyte Interfaces Derived from Aggregation-Dominated Electrolyte

Shu Yang[a], Xianshu Wang[c], Ruimin Li[b], Yiming Zhou[a], Haonan Huang[d], Mengyuan Zhou[a], Yunyun Gao[a], Wanyu Zhao[b], Yukui Gao[a], Zhenghui Pan[a*], Xiaowei Yang[b*]

a. School of Materials Science and Engineering, Tongji University, Shanghai, 201804, China.

b. School of Chemistry and Chemical Engineering, Shanghai Jiao Tong University, Shanghai, 200240, China.

c. National and Local Joint Engineering Research Center of Lithium-ion Batteries and Materials Preparation Technology, Kunming University of Science and Technology, Kunming, 650093, China.

d. School of Chemistry, South China Normal University, Guangzhou, 510006, China.

Email addresses: zhenghuipan@tongji.edu.cn; yangxw@sjtu.edu.cn

Experimental Section

Electrolyte preparation and cell assemble

Baseline electrolytes were prepared by dissolving 0.09 M calcium bis(trifluoromethanesulfonyl)imide ($Ca(TFSI)_2$, >99.50%, DoDoChem) in fluoroethylene carbonate (FEC, Aladdin, > 99.0%)/ dimethoxyethane (DME) (1:2 by weight, Aladdin, >99.5%). 1.71 M Lithium tetrafluoroborate ($LiBF_4$, Aladdin, > 99.0%) was added into the baseline electrolyte to prepare the CTFSI-LBF electrolyte. EC/PC-based electrolyte was prepared by dissolving 0.1 M $Ca(TFSI)_2$ in ethylene carbonate (EC, Aladdin, > 99.0%)/ propylene carbonate (PC, Aladdin, >99.7%) (1:2 by weight, Aladdin, >99.5%). DME-based electrolyte was prepared by dissolving 0.1 M $Ca(TFSI)_2$ in DME solvent. To prepare prussian blue analogue (PBA) cathode, a slurry was prepared by mixing 80 wt.% PBA (Ningbo Jinhe New Materials Co., Ltd), 10 wt.% acetylene black (AB, Shenzhen Kejing Star Technology Co., Ltd) and 10 wt.% polyvinylidene fluoride (PVdF, Shenzhen Kejing Star Technology Co., Ltd) in N-methyl pyrrolidone (NMP) solvent. The slurry was coated onto aluminum foil with an average mass loading of 2.5 mg cm^{-2}. The PBA electrodes were dried at 70 °C for 12 h under vacuum and then cut into discs with a diameter of 12 mm. Ca//Ca symmetric cells were assembled with the two Ca electrodes (diameter =16 mm, thickness =1.0 mm), a glass fiber separator (Whatman GF/D) and 100 μL electrolyte. Ca electrodes recovered from Ca symmetric cells after five cycles were sandwiched between two stainless steels (SS) to construct a blocking electrode configuration. Ca//Cu cells were assembled with the Ca electrodes (diameter = 16 mm, thickness = 1.0 mm), Cu foil (diameter =16 mm), a glass fiber separator (Whatman GF/D) and 80 μL electrolyte. PBA//Ca coin-type cells were assembled with PBA electrode and Ca electrode (diameter =16 mm, thickness =0.05 mm) with 80 μL electrolyte. The N/P ratio of PBA//Ca cell is 23. Note that Electrolyte preparation and cell assembly/disassembly were performed in a glove box (Vigor, Germany), where the contents of water and oxygen were controlled below 0.1 ppm.

Electrochemical characterization

Ca//Ca symmetric cells were charging/discharging at a current density of 0.02 mA cm^{-2} and a capacity of 0.02 mA h cm^{-2} at room temperature, which was performed by the BTSDA battery testing system (China). The electrochemical impedance spectroscopy (EIS) was carried out on Bio-Logic VMP3, with frequencies from 100 kHz to 10^{-1} Hz with a potential amplitude of 5 mV. The

electrochemical oxidation activity of electrolytes was determined by linear sweep voltammetry (LSV) from open circuit potential to 5 V at a scanning rate of 1 mV s^{-1}. Cyclic voltammetry (CV) was conducted on Ca//Cu 2032-type coin cells between −1.5 and 2.5 V at a scan rate of 5 mV s^{-1} using Cu substrate as working electrode and Ca electrode as reference/counter electrode. The voltage responses under a current of 5 mA were recorded after standing for 200 s at OCV, and the electrical resistivity was calculated based on Eq. (1), in which U refers to the voltage and I refers to the current.

$$R = \frac{U}{I} \qquad \text{Eq. (1)}$$

For the galvanostatic intermittent titration (GITT) measurement, the Ca//Ca symmetric cells were charged at constant current (0.04 mA) for 10 min, with a sand's time of 30 min. The ionic conductivities (σ) of electrolytes were measured using platinum black conductance electrodes from 25 to 75 ℃ in the programmable high-temperature test chamber, in which the conductivity cell constant is 1.008. The calcium-ion transference number ($t_{Ca^{2+}}$) was obtained by the combination of EIS and potential chronoamperometry (CA) using Ca//Ca cells. The initial current (I_0) and steady current (I_s) was determined by CA characterization on Bio-Logic VMP3 at a constant voltage of 10 mV (ΔV). The value of $t_{Ca^{2+}}$ was calculated by Eq. (2).

$$t_{Li^+} = \frac{I_S(\Delta V - I_0 R_0)}{I_0(\Delta V - I_S R_S)} \qquad \text{Eq. (2)}$$

Galvanostatic charging/discharging of Ca symmetric cells at various currents from 5 to 70 μA was performed to measure the overpotential and calculate the exchange current density (i_0) using Eq. (3), in which η is the total overpotential, F is Faraday's constant, and R is the standard gas constant.

$$i = i_0 \frac{zF\eta_{tot}}{RT} \qquad \text{Eq. (3)}$$

Physicochemical characterization

For the physicochemical characterizations, the cycled cells were disassembled, and then the recovered electrodes were rinsed three times with DME solvent to remove the residual electrolyte, followed by drying in the glove box overnight. The morphology of the Ca anode and corresponding Ca deposits were observed with scanning electron microscopy (SEM, FEI–quanta 250, America). The time-of-flight secondary ion mass spectroscopy (TOF-SIMS) was performed using a TOF-SIMS 5-100 (ION TOF) with a Bi^{3+} gun at 50 keV. For surface analysis, the flood gun is tun to deliver Bi^{3+}

primary ions with a 50×50 μm^2 raster size. Depth profile experiments are carried out using previous conditions for surface analysis ($Bi^{3+,}$ 50×50 μm^2 raster size) and a 2 kV Cs^+ gas gun for etching (with a sputtered area of 200×200 μm^2). In-depth X-ray photoelectron spectroscopy (XPS, AXIS SUPRA, Japan) spectra were conducted with a monochromatized Al Kα X-ray source (beam diameter 200 μm, X-ray power 50 W). Sputter etching was performed using an Ar^+ gun at 2 kV.

Theoretical calculations

Density functional theory (DFT) calculations for binding energy were carried out using the Gaussian 16 package. The optimum structures were performed by B3LYP in combination with the 6-311++G basis set. The binding energy (E_b) of different clusters is calculated as:

$$E_b = E_{custer} - E_m - E_{Ca}^{2+}$$

where cluster is the free energy of Ca^{2+}-M (M = $CaC_4O_3H_8$, $CaC_3O_3H_8$, $CaC_4O_6H_4$ and CaF_2). First-principles calculations were executed using the Vienna Ab initio Simulation Package (VASP)

Molecular dynamics (MD) simulations were carried out by using the Large-scale Atomic/Molecular Massively Parallel Simulator with OPLS-AA force field.[1] The compositions of electrolytes are 420 FEC, 10 $Ca(TFSI)_2$, 990 DME; 420 FEC, 10 $Ca(TFSI)_2$, 990 DME, 190 $LiBF_4$. OPLS-AA parameters with 1.14*CMIA partial atomic charges were generated by LigParGen for the DME, FEC molecules.[2,3] The systems were then pre-equilibrated via isothermalisobaric (NPT) ensemble at 330 K for 2 ns. Another canonical (NVT) ensemble runs with simulation time of 5 ns and the last 1 ns was performed to obtain the structure of electrolyte.

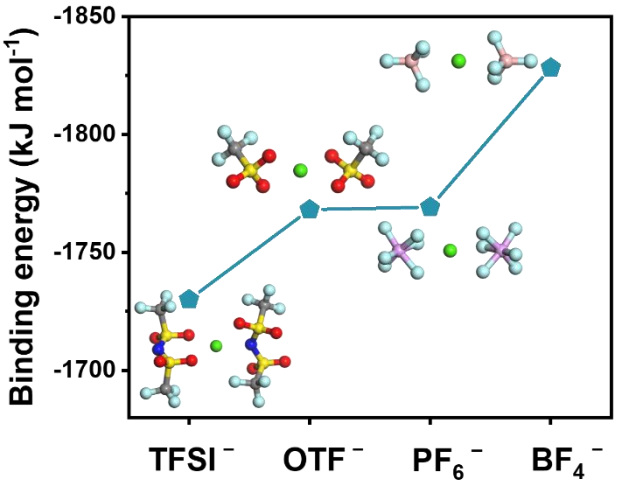

Fig. S1 Calculated binding energies (E_b, kJ mol^{-1}) between Ca^{2+} and $TFSI^-$, OTF^-, PF_6^- or BF_4^- anion.

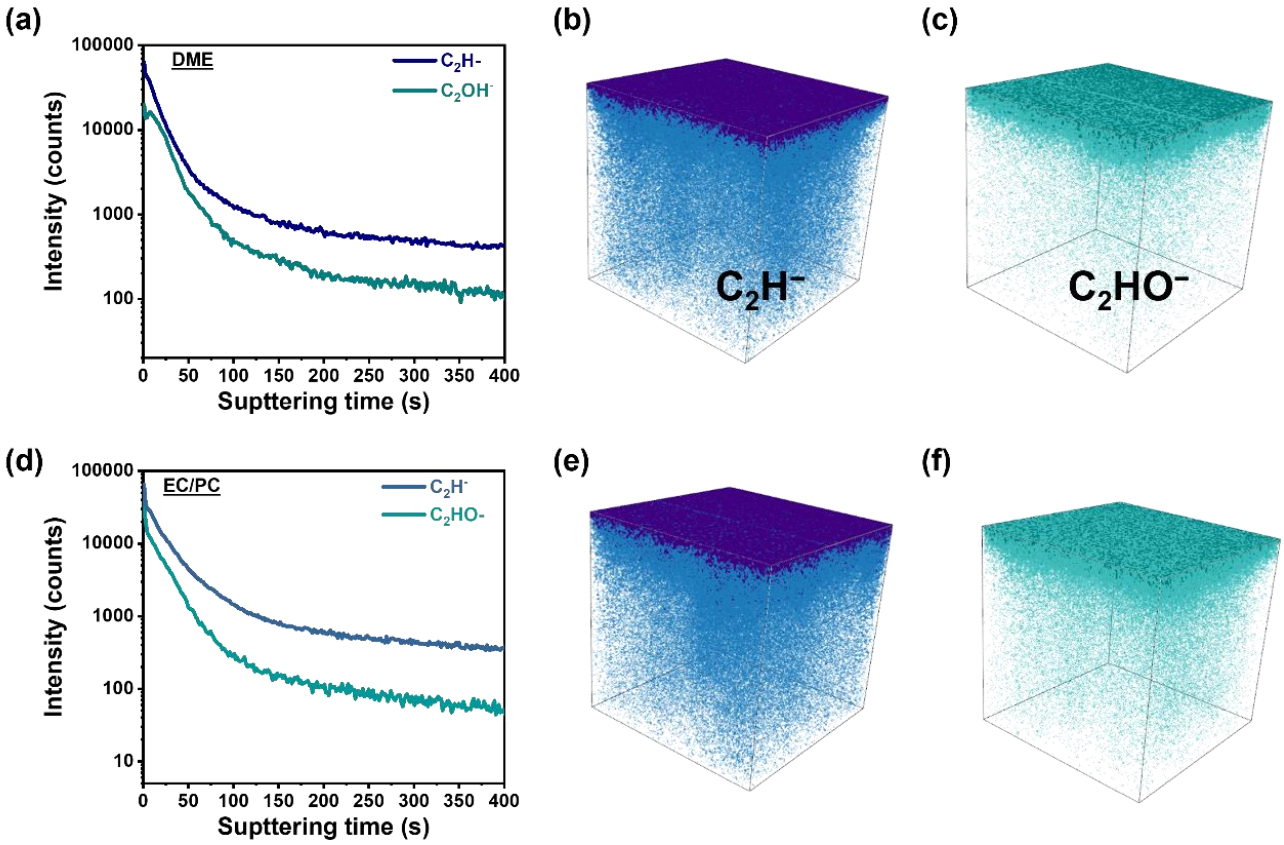

Fig. S2 Intensity sputter profiles and corresponding 3D Render overlay of various species in SEI formed in (a-c) DME- and (d-f) EC/PC-based electrolytes.

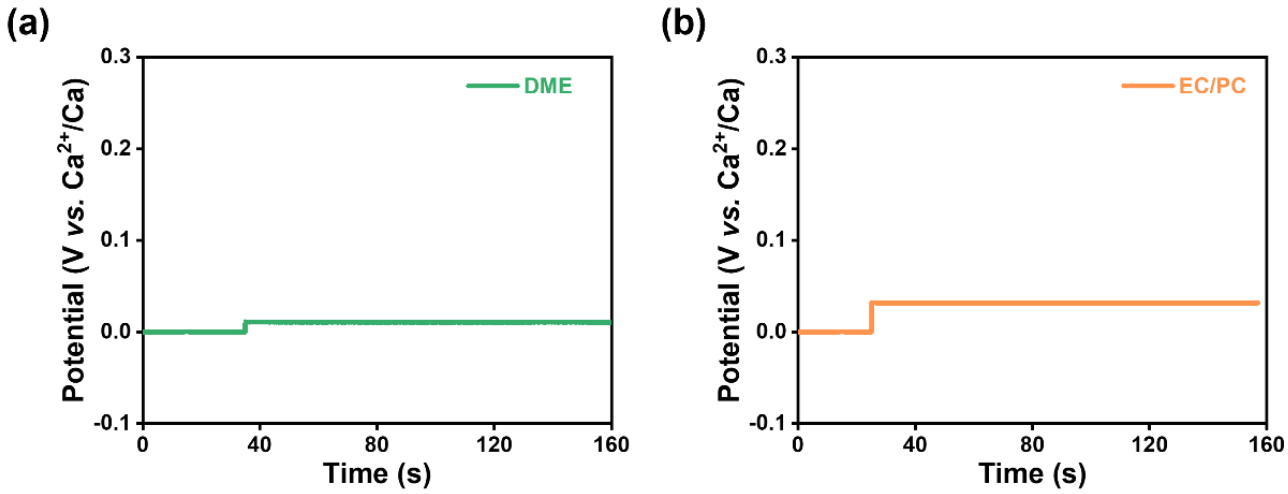

Fig. S3 Voltage response curves of DME and EC/PC electrolytes at a current of 5 mA after 120 s standing at OCP.

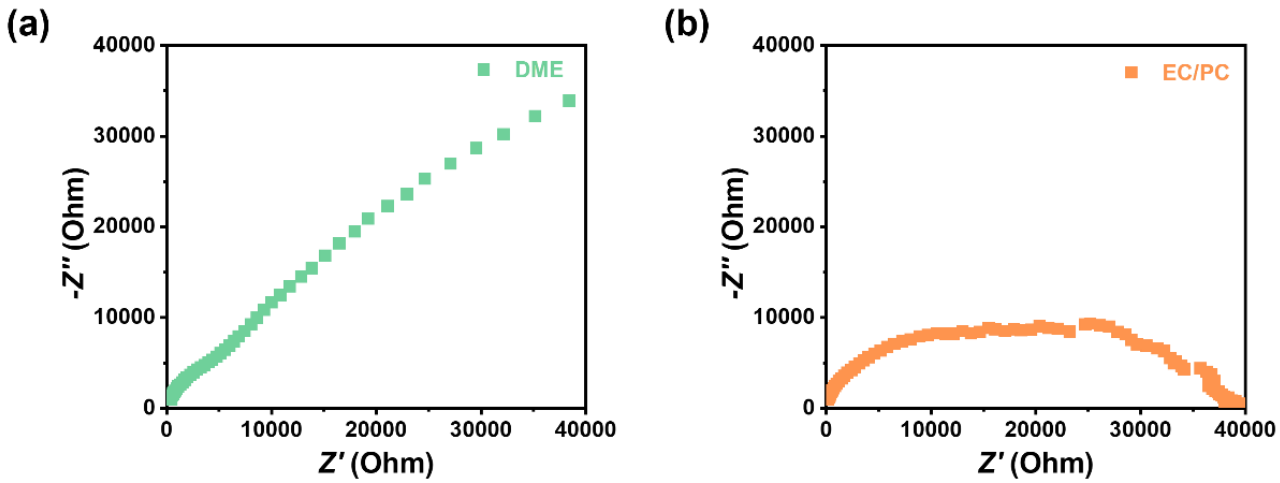

Fig. S4 EIS plot for measuring ion transport resistance, measured at 10^5-0.01 Hz with 5 mV amplitude.

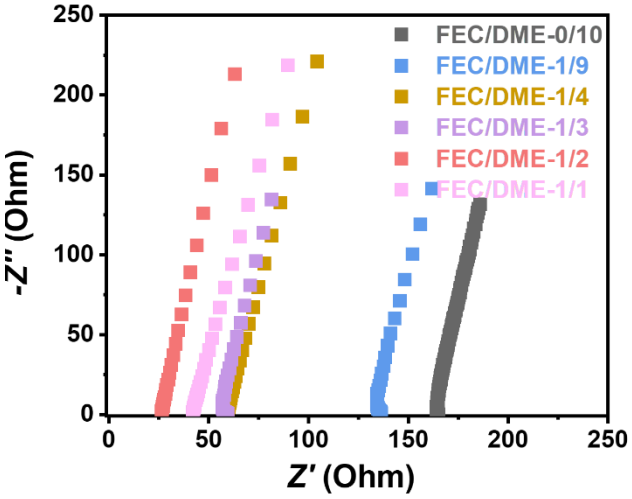

Fig. S5 EIS plots for SS//SS cells in FEC/DME mixture electrolytes with the concentration of $Ca(TFSI)_2$ salt is 0.09 M at room temperature, measured at 10^5-0.1 Hz with 5 mV amplitude.

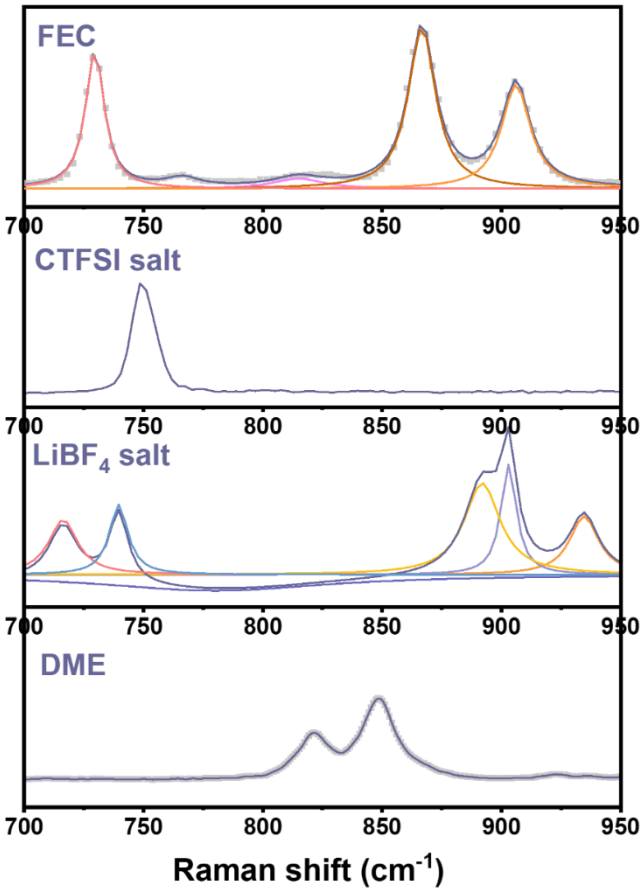

Fig. S6 Raman spectra of various solvents and salts.

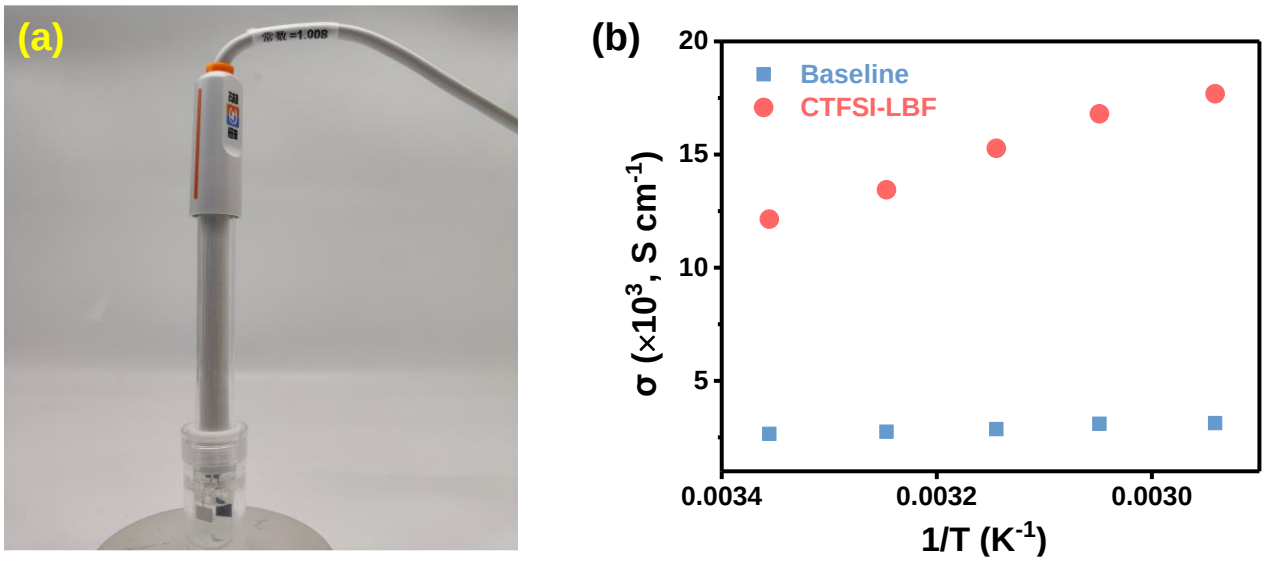

Fig. S7 Electrolyte conductivities at different temperatures using a conductivity electrode, whose conductivity constant is 1.008.

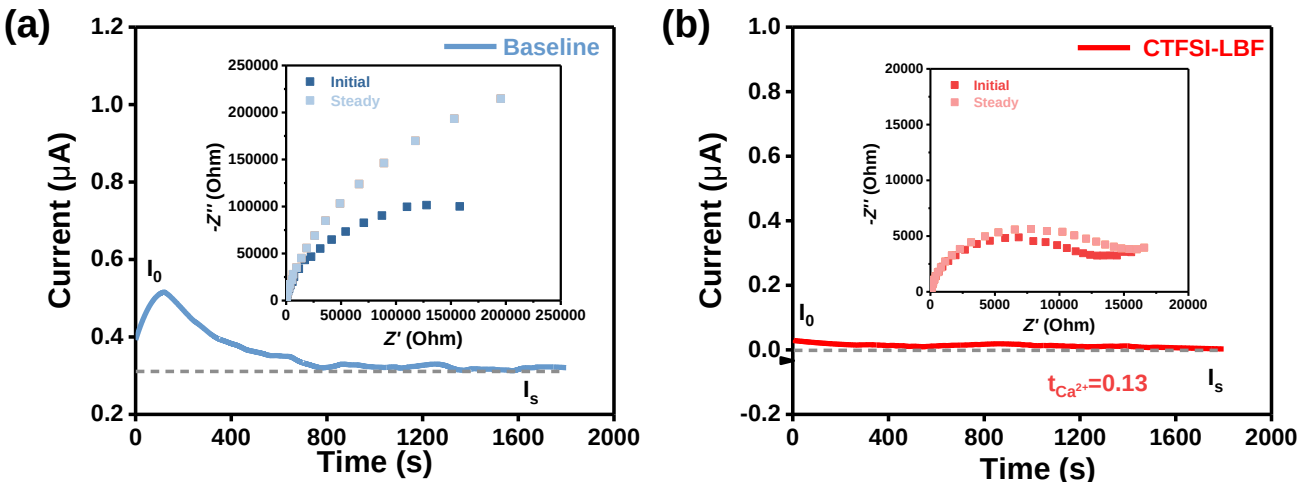

Fig. S8 Potential chronoamperometry (CA) curves of Ca symmetric cells in (a) baseline and (b) CTFSI-LBF electrolytes, the applied potential (ΔV) was 10 mV (inset image is EIS plots of Ca symmetric cells before and after CA measurements).

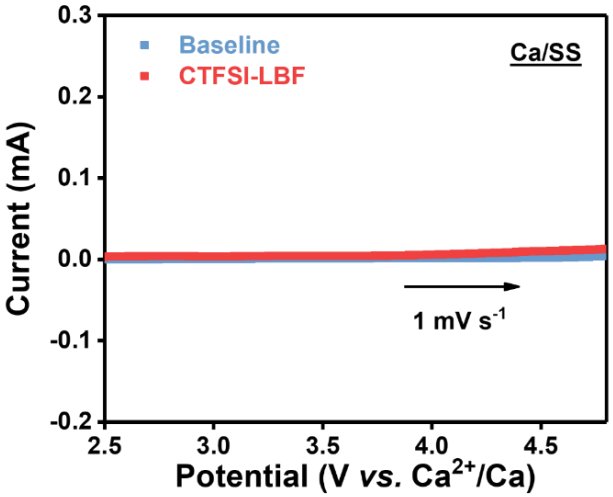

Fig. S9 LSV of Ca//SS cells from OCP to 4.8 V in various electrolytes at a scan rate of 1 mV s^{-1}.

The physical properties of electrolytes themselves are essential factors in their practical application. A platinum black conductance electrode was used to measure electrolyte conductivity accurately. Compared to the ionic conductivity of the baseline system, as shown in Fig. S7, which is only 2.6 mS cm^{-1} at room temperature (25 ˚C), the conductivity of CTFSI-LBF electrolyte exhibits a considerable increase (12.1 mS cm^{-1}). Besides, the calcium-ion transference number (t_{Ca}^{2+}) was determined as 0.13 based on the method described by Abraham et al. and Eq. (2) (Fig. S8), which is conducive to minimizing concentration polarization and avoiding Ca^{2+} transport through the electrolyte as a rate-limiting step. The electrochemical stability is also a crucial factor in evaluating the practicability of electrolyte materials. LSV was conducted on Ca//SS coin-type cells to investigate the electrochemical stability of different electrolytes. CTFSI-LBF electrolyte exhibits a wide electrochemical window of over 4.5 V (Fig. S9, oxidative current < 10 μA), suggesting that the improved cycling stability is not at the expense of the oxidative stability of the electrolyte.

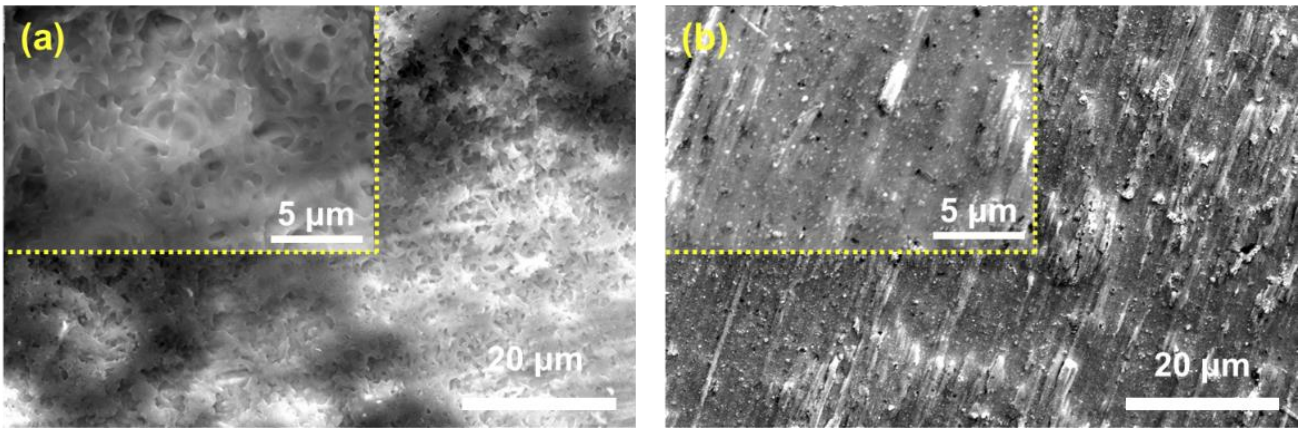

Fig. S10 Top-view SEM images of Cu electrodes after 10 cycles cycled in (a) baseline and (b) CTFSI-LBF electrolytes.

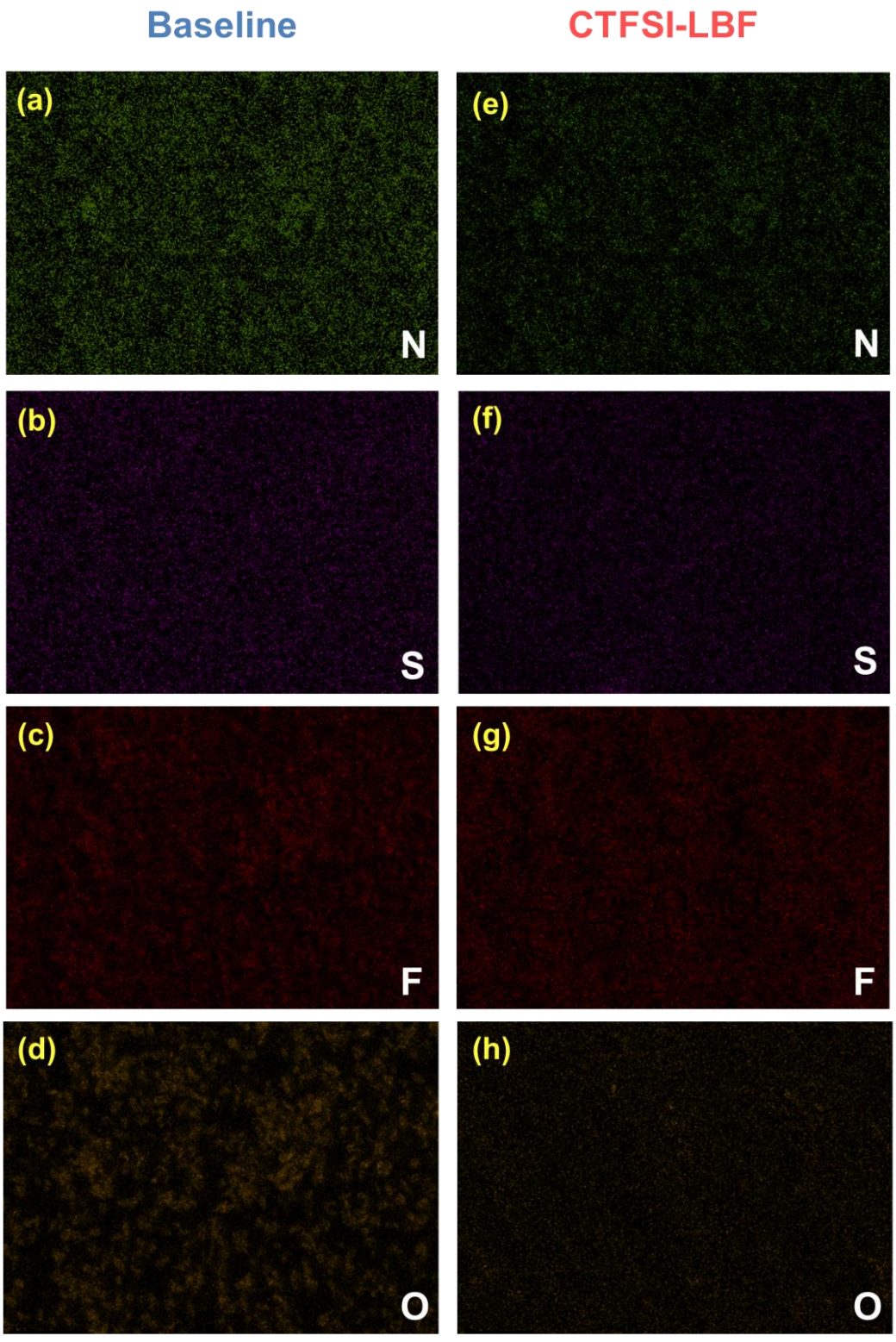

Fig. S11 EDS mapping (N, S, F and O) of the Cu substrates after constant potential deposition process at −0.3 V for 10 h using (a-d) baseline and (e-h) CTFSI-LBF electrolytes.

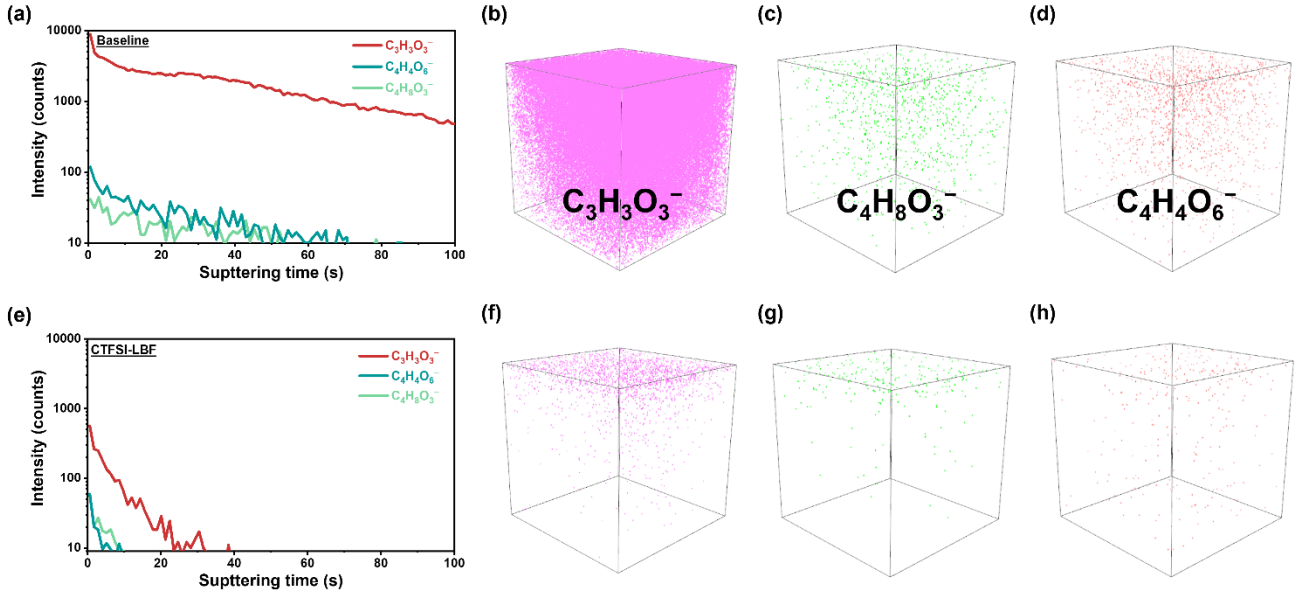

Fig. S12 Intensity sputter profiles and corresponding 3D Render overlay of various species in SEI formed in (a-d) baseline and (e-h) CTFSI-LBF electrolytes.

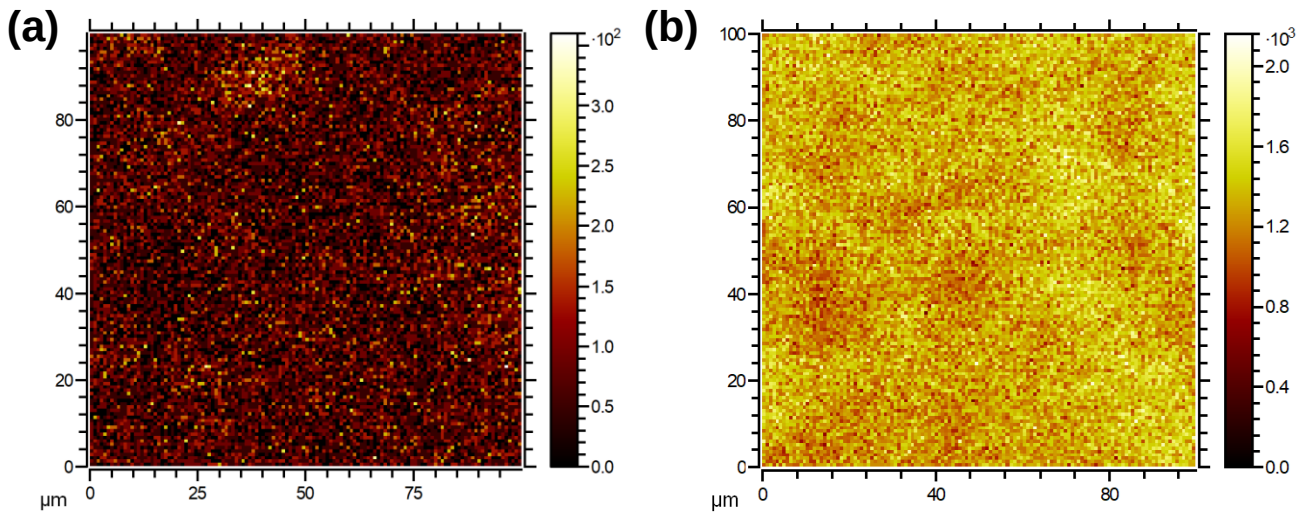

Fig. S13 Distribution map of F-containing species in SEI formed in (a) baseline and (b) CTFSI-LBF electrolytes.

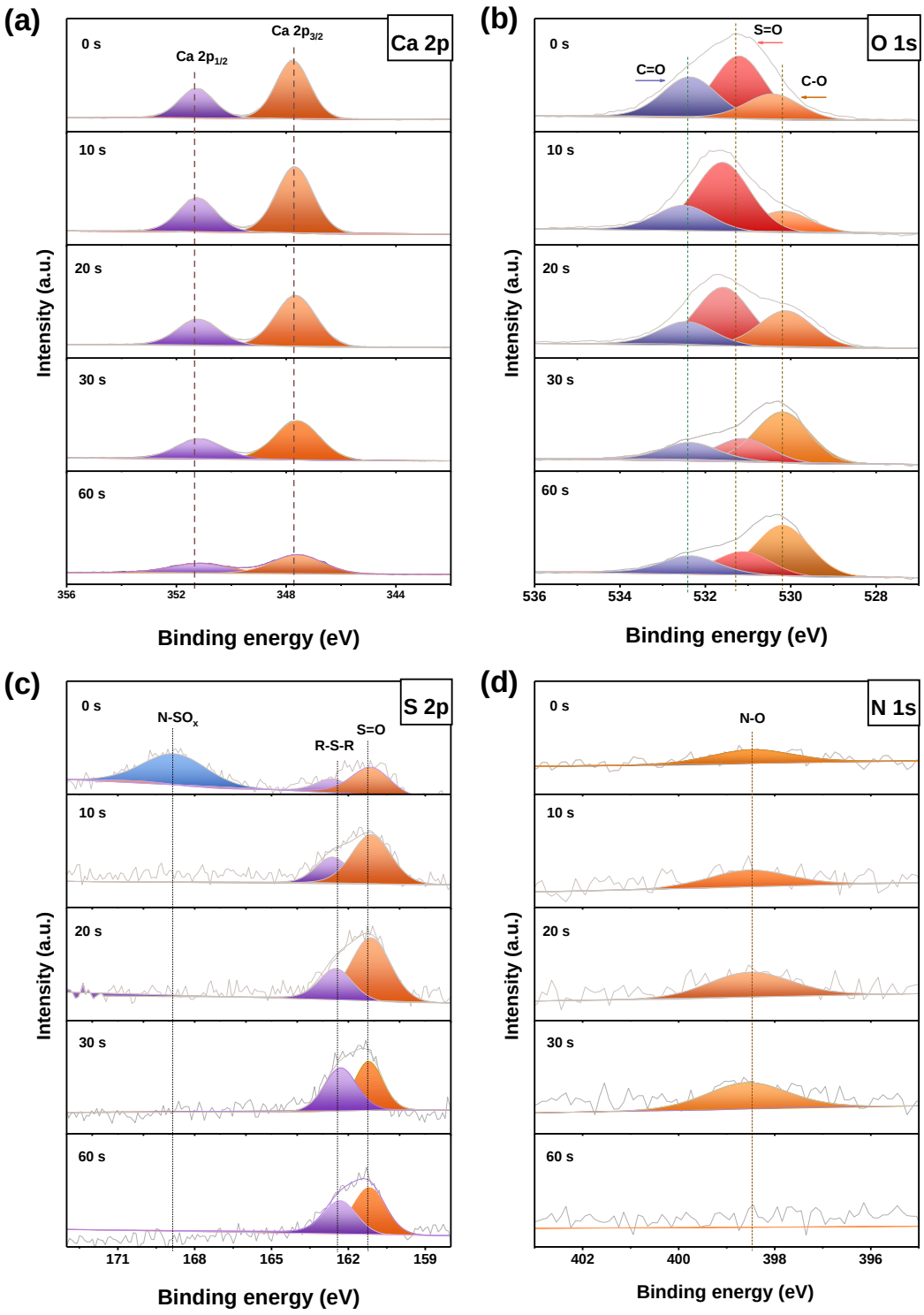

Fig. S14 XPS spectra of (a) Ca 2p, (b) O 1s, (c) S 2p and (d) N 1s of Cu substrate taken from Ca//Cu cell after 10 cycles in baseline electrolyte.

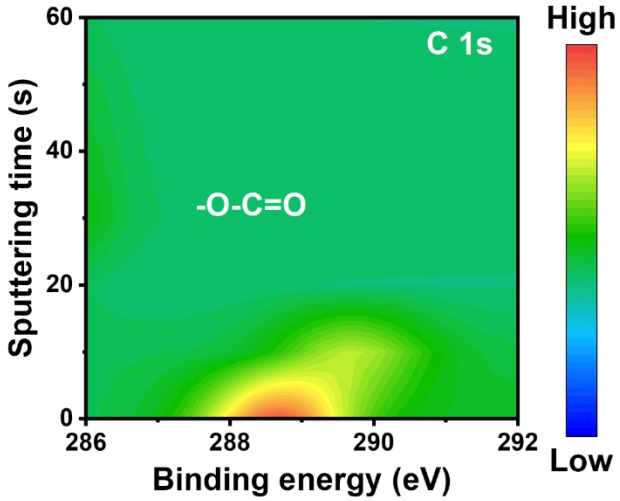

Fig. S15 C 1s in-depth XPS spectrum of SEI layer on Cu electrodes recovered from Ca//Cu cells after cycle 10 cycles in baseline electrolyte.

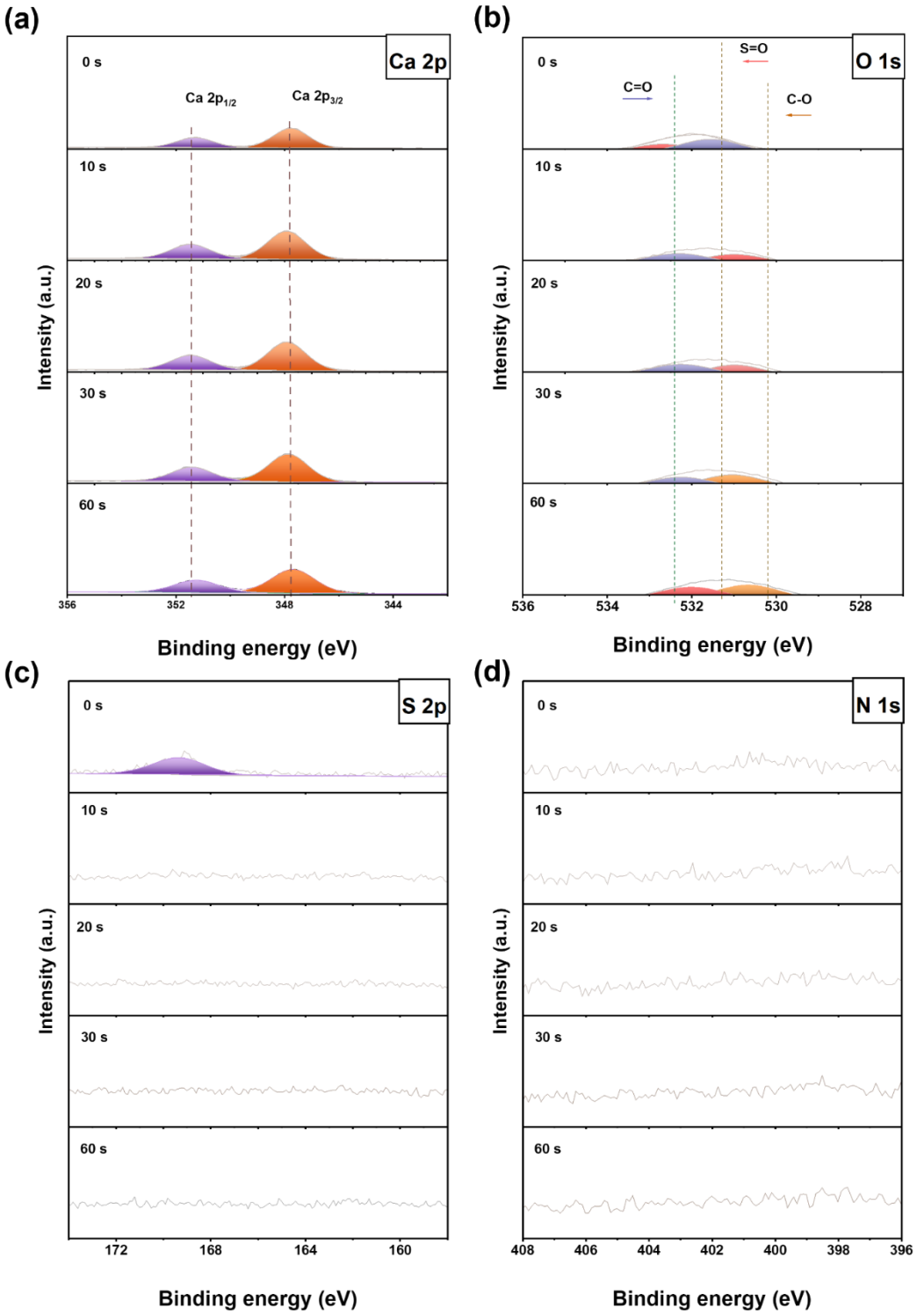

Fig. S16 XPS spectra of (a) Ca 2p, (b) O 1s, (c) S 2p and (d) N 1s of Cu substrate taken from Ca//Cu cell after 10 cycles in CTFSI-LBF electrolyte.

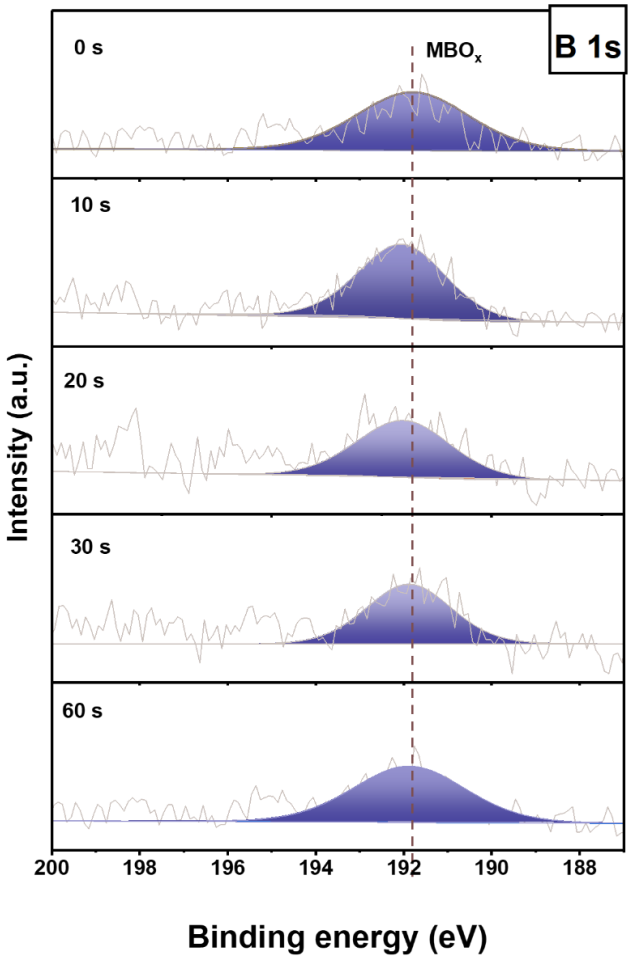

Fig. S17 XPS spectra of B 1s of Cu substrate taken from Ca//Cu cell after 10 cycles in CTFSI-LBF electrolyte.

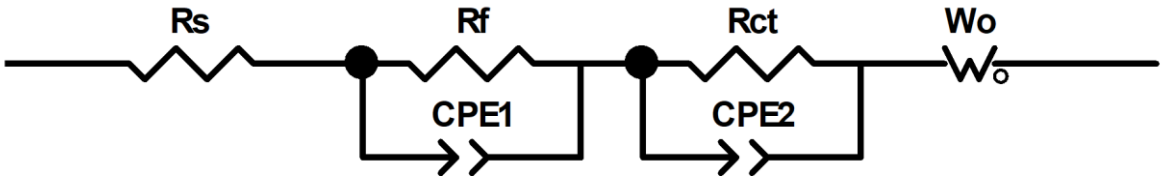

Fig. S18 Equivalent circuit model adopted to fit the Nyquist plots.

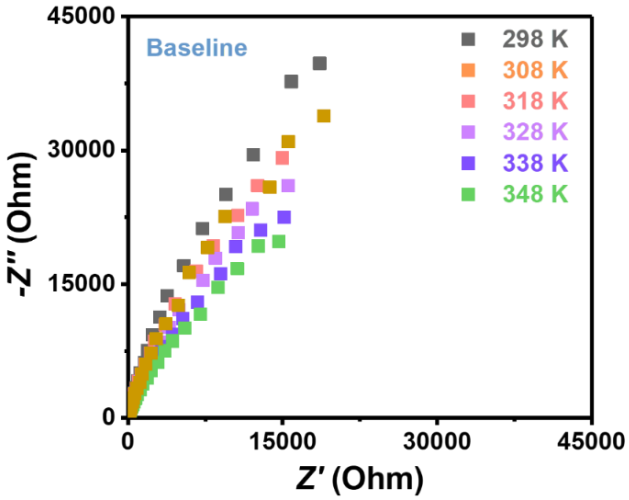

Fig. S19 Temperature-dependent EIS plots of Ca symmetric cells in baseline electrolyte.

In baseline electrolytes, too high cell resistance to estimate the E_a (Fig. S19), which is caused by an organic-rich passivation layer derived by electrolyte decomposition. Compared with it, the EIS results for CTFSI-LBF electrolyte contain a semicircle at high and medium-frequency ranges, together with a straight line at a low-frequency range, which is called interfacial impedance (R_f), charge transfer impedance (R_{ct}) and Warburg impedance (W_o), respectively, reflecting the kinetics of Ca^{2+} transport and diffusion (Fig. S18).

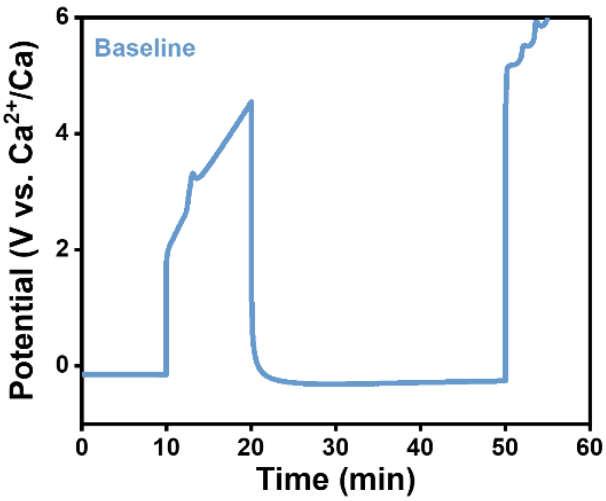

Fig. S20 GITT curves in baseline electrolyte with a current density of 0.02 mA cm^{-2} applied for 10 minutes with 30 minutes of rest between pulses during the plating/stripping process.

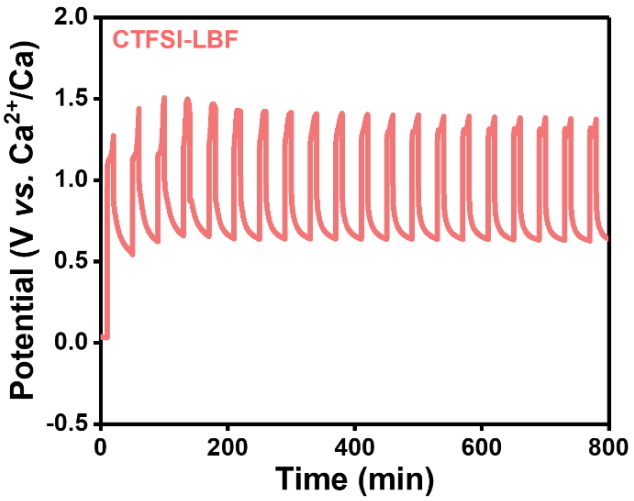

Fig. S21 GITT voltage curves of Ca anode in CTFSI-LBF electrolyte with a current density 0.02 mA cm^{-2} applied for 10 minutes with 30 minutes of rest between pulses during the plating/stripping process.

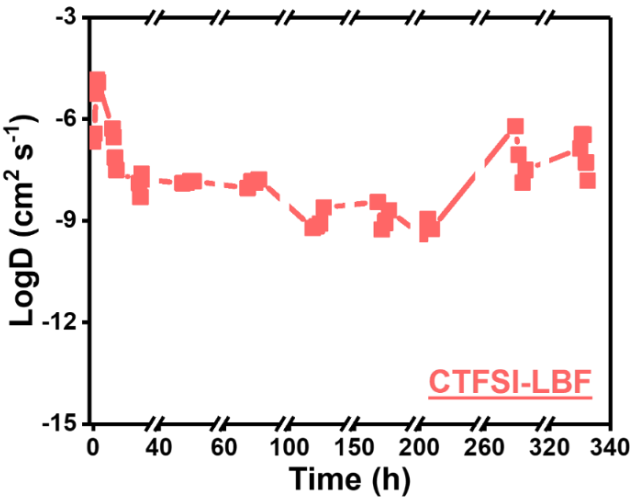

Fig. S22 Calculation of Ca^{2+} diffusion coefficient (D_{Ca}^{2+}) from GITT measurements in CTFSI-LBF electrolyte.

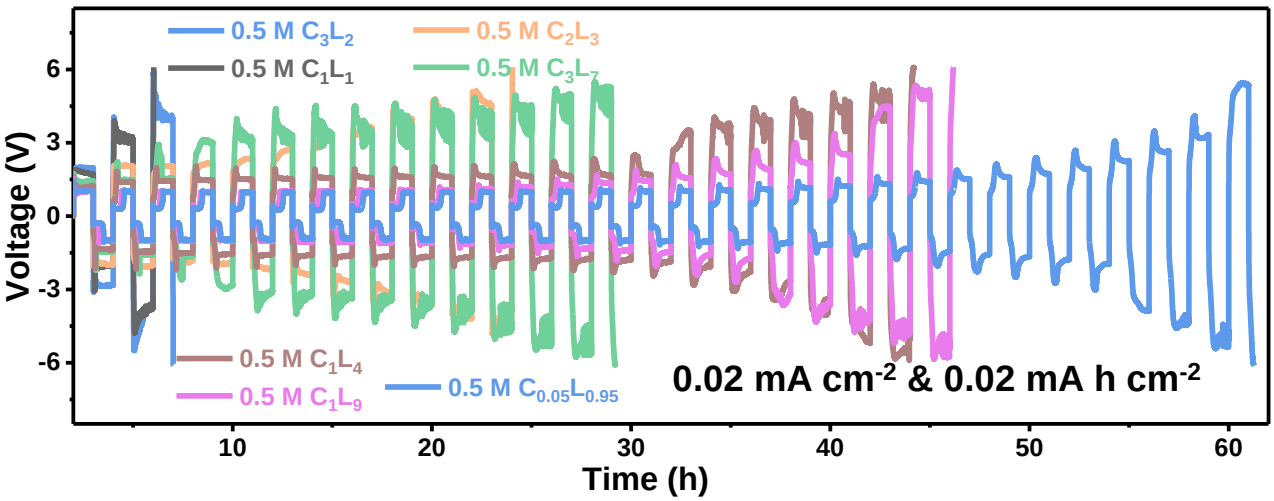

Fig. S23 Time-voltage curves of Ca symmetric cells cycled in dual-salt mixture electrolytes, with a current density of 0.02 mA cm^{-2} and capacity density of 0.02 mA h cm^{-2}.

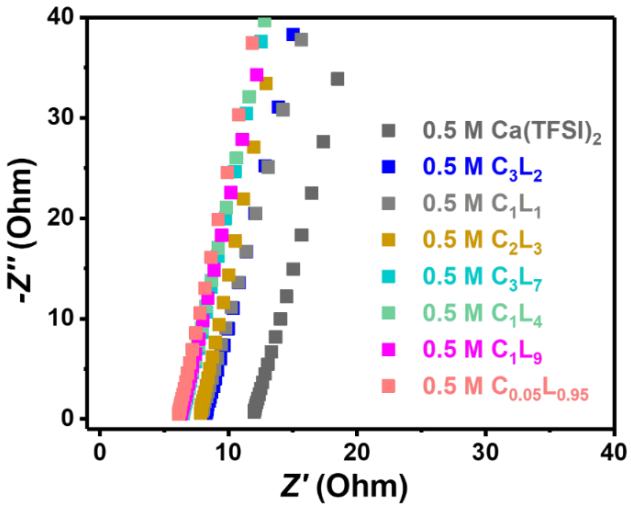

Fig. S24 Electrochemical impedance spectra (EIS) for stainless steel (SS)/SS cells in Ca-Li dual-salt mixture electrolytes at room temperature, measured at 10^5-0.1 Hz with 5 mV amplitude.

.

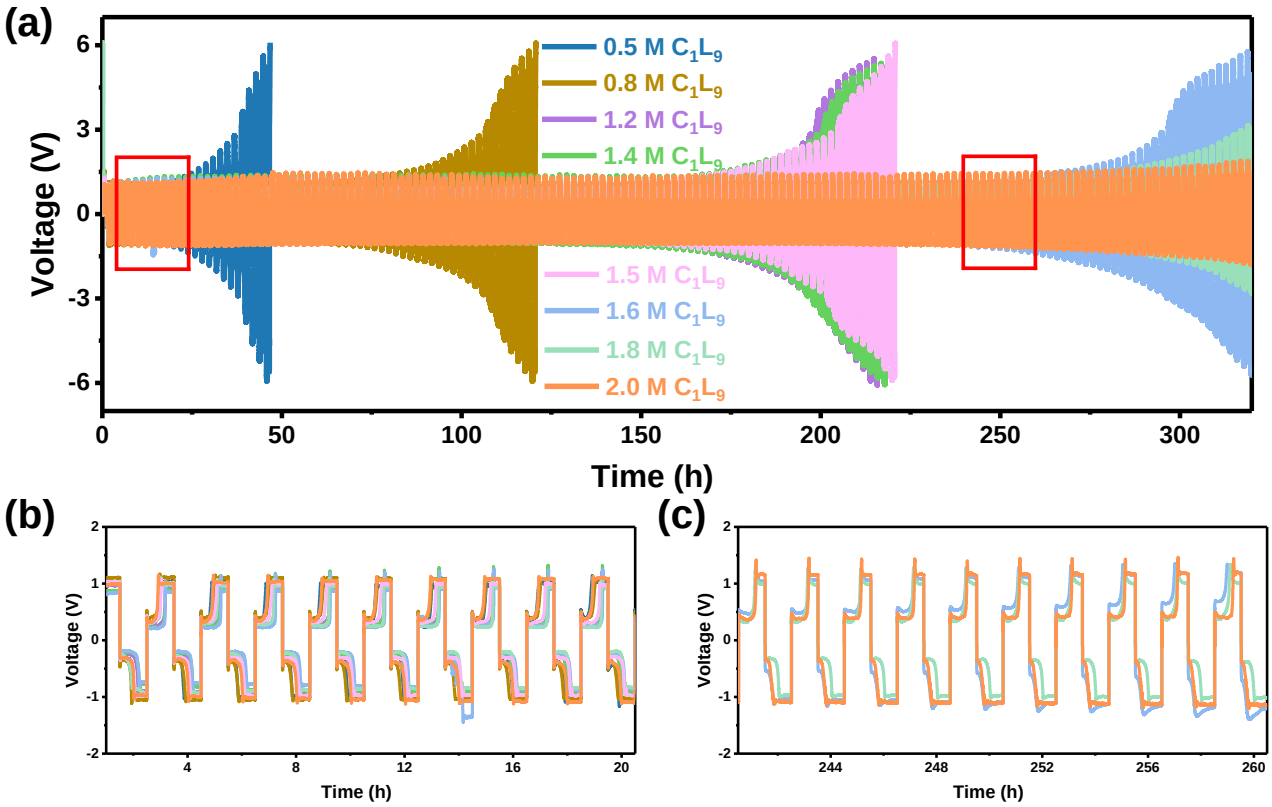

Fig. S25 Time-voltage curves of Ca symmetric cells cycled in Ca-Li dual-salt mixture electrolytes with a constant proportion of C_1L_9, with a current density of 0.02 mA cm^{-2} and capacity density of 0.02 mA h cm^{-2}. Voltage-time profiles during (b) 2-22 h and (b) 242-262 h in various electrolytes.

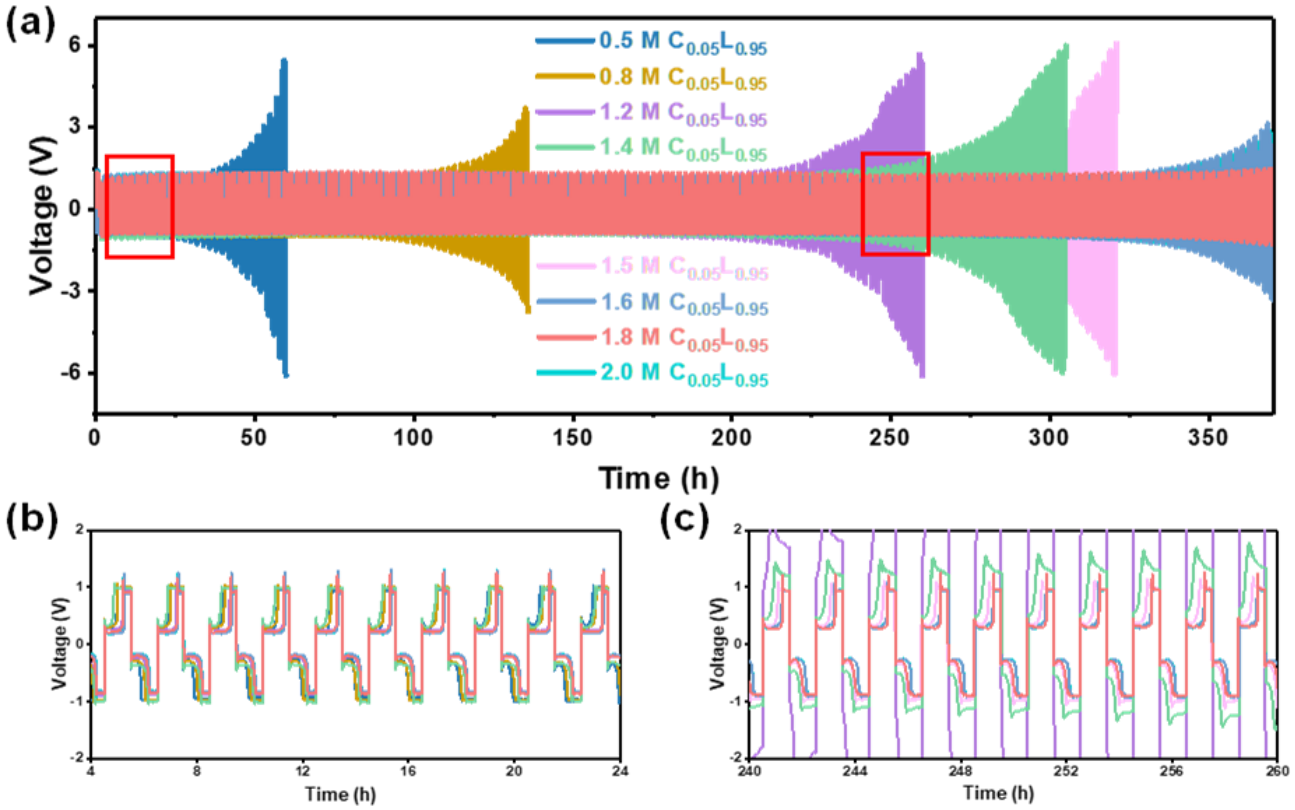

Fig. S26 (a) Time-voltage curves of Ca symmetric cells cycled in Ca-Li dual-salt mixture electrolytes with a constant proportion of CTFSI-LBF, with the current density of 0.02 mA cm^{-2} and capacity density of 0.02 mA h cm^{-2}. Voltage-time profiles during (b) 4-24 h and (c) 240-260 h in various electrolytes.

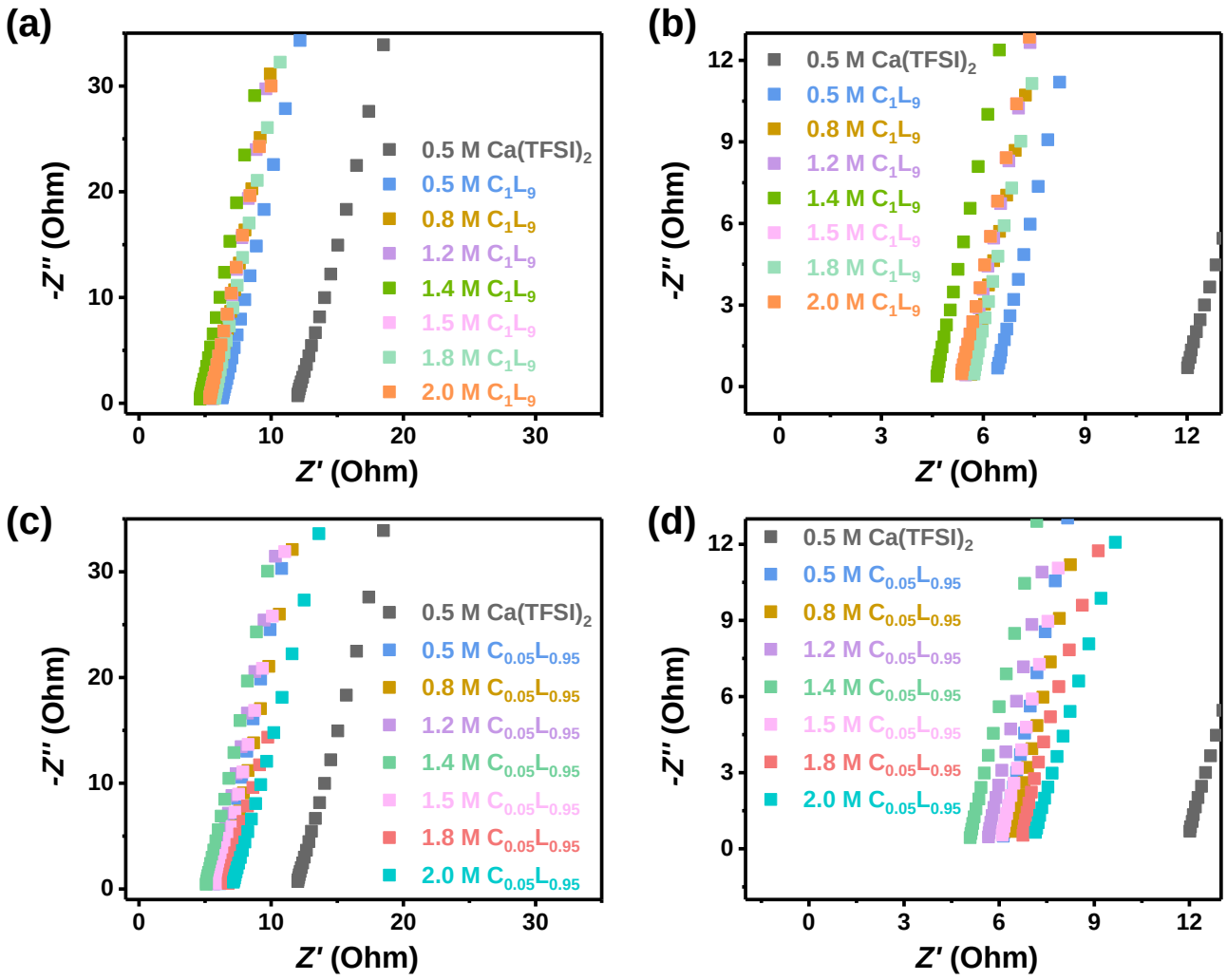

Fig. S27 EIS plots for SS/SS cells in Ca-Li dual-salt mixture electrolytes at room temperature, measured at 10^5-0.1 Hz with 5 mV amplitude.

The voltage evolution of Ca//Ca symmetric cells was assembled to investigate the compatibility of various electrolytes with Ca anode. Firstly, the cycling performance in various electrolytes was compared to find the optimal ratio of Li salt to Ca salt (Fig. S23). As shown in Fig. S24 and S25, it can be inferred that the interfaces formed in electrolytes containing lower concentrations of salts are not sufficiently stable. At the same time, higher-concentrated salt shows a higher polarization (Fig. S26(b-c)), possibly due to increased electrolyte viscosity and reduced conductivity (Fig. S27(a-b)). As BF_4^- is added to $Ca(TFSI)_2$-based electrolyte, the cycling performance is improved with the best CTFSI-LBF electrolyte. However, the cycling stability no longer varies linearly with the ionic conductivity of

electrolytes (Fig. S27(c-d)). Significantly improved cycle stability yet slightly lower electrolyte conductivity further suggests that the effects of CTFSI-LBF electrolyte on cell stability are dominated by inorganic-rich SEI containing fluoride and borate rather than the increase of ionic conductivity.

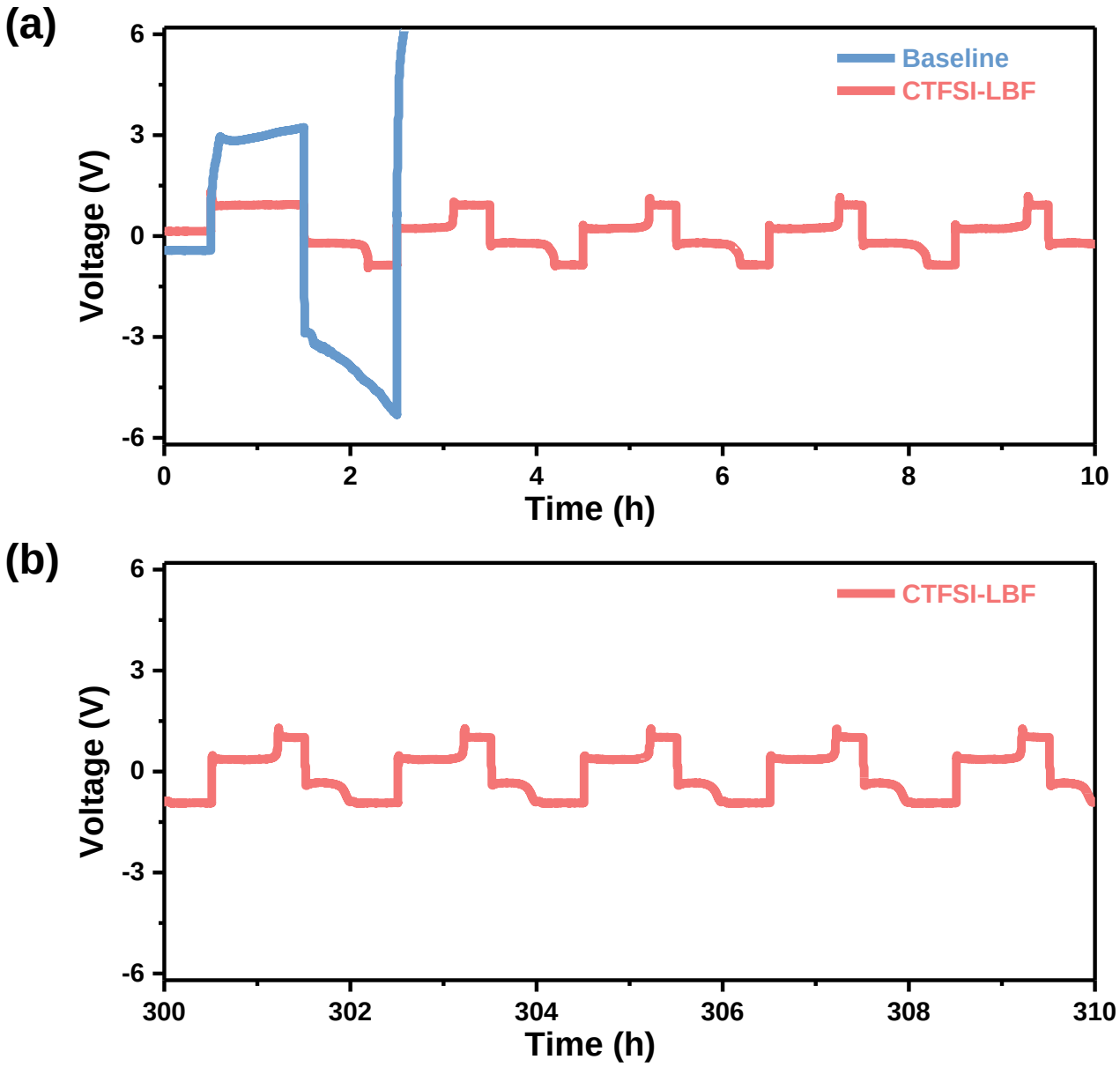

Fig. S28 Voltage-time profiles during (a) 0-10 h and (b) 300-310 h in various electrolytes.

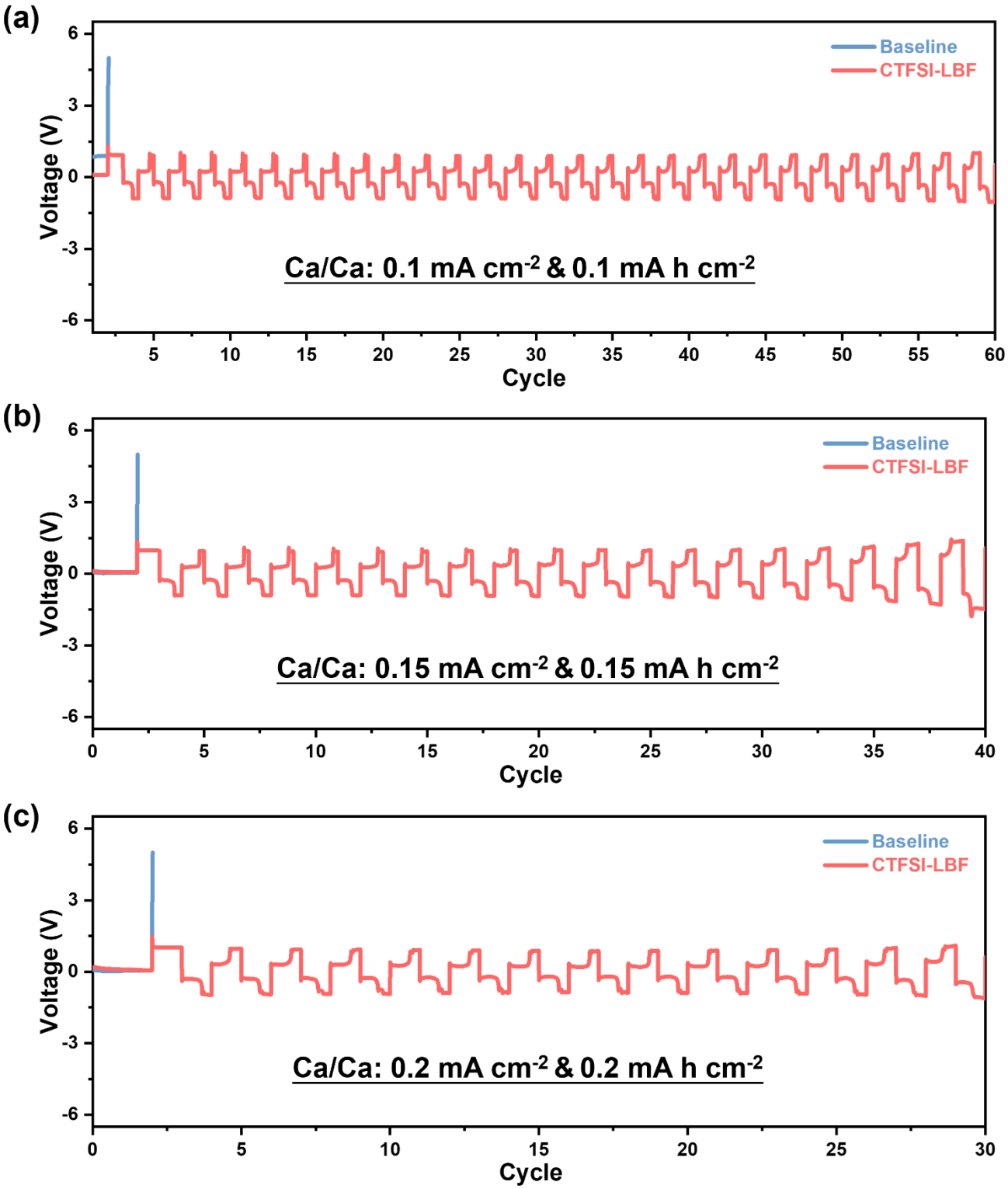

Fig. S29 Cyclic stability of Ca//Ca symmetric cells with various capacity density.

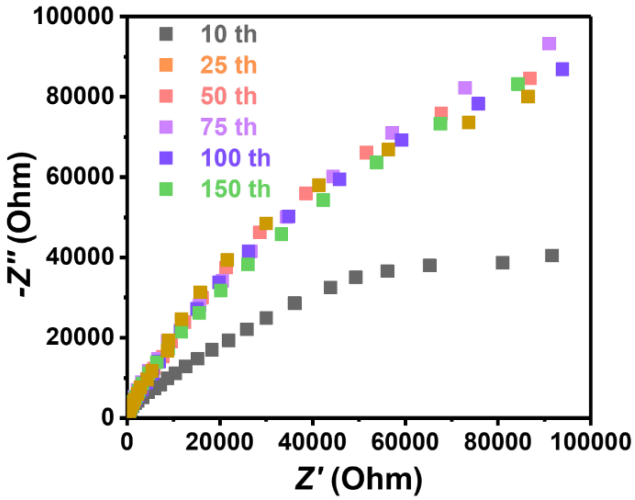

Fig. S30 EIS plots of Ca symmetric cell after various cycles in CTFSI-LBF electrolyte.

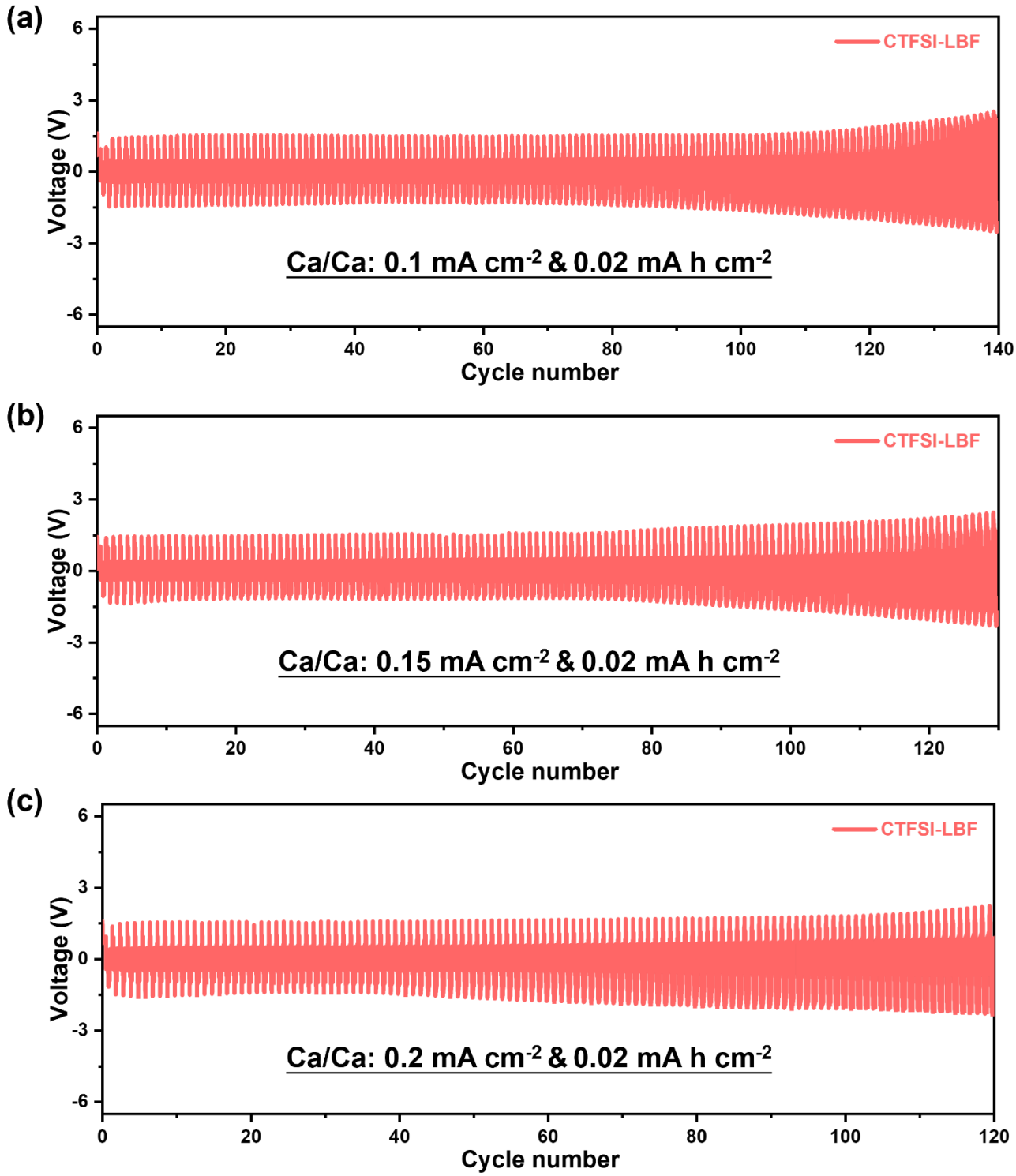

Fig. S31 Cyclic stability of Ca symmetric cells in various electrolytes at various current densities.

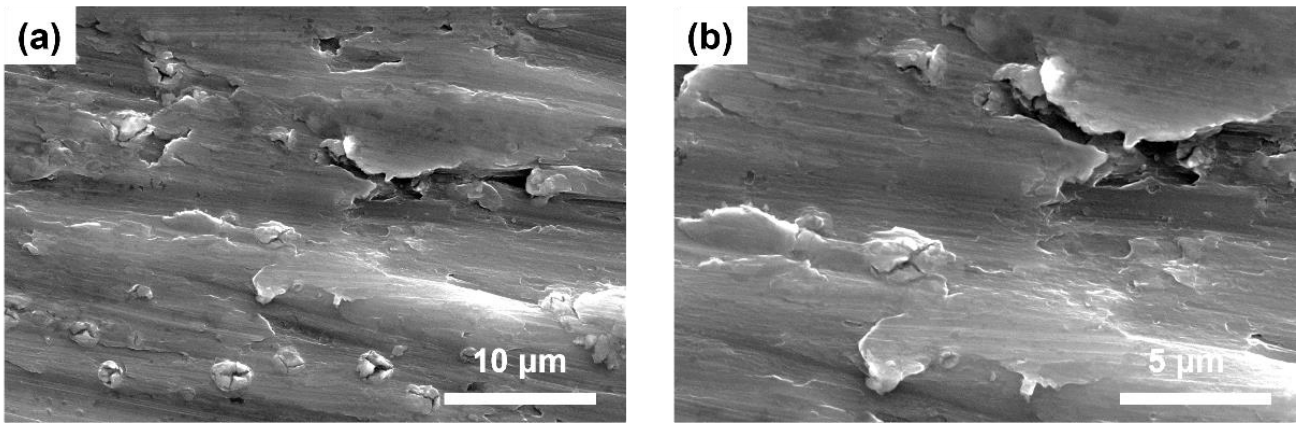

Fig. S32 SEM images for the fresh Ca metal anode.

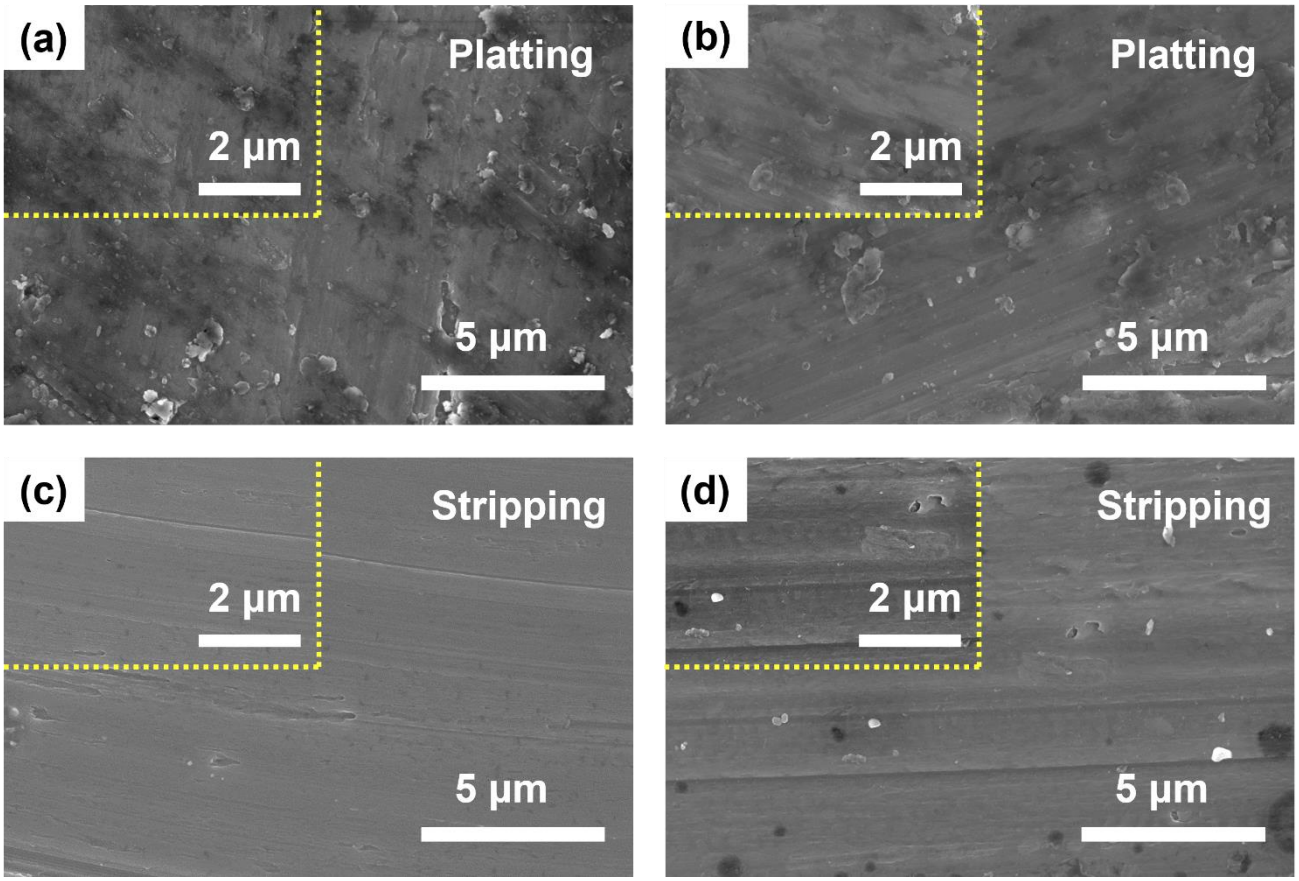

Fig. S33 SEM images of Ca metal anodes recovered from Ca//Ca symmetric cells after (a, b) plating or (b, d) stripping at (a, c) 0.06 mA cm^{-2} and (b, d) 0.15 mA cm^{-2} for 0.2 mA h, respectively (inset showing enlarged views).

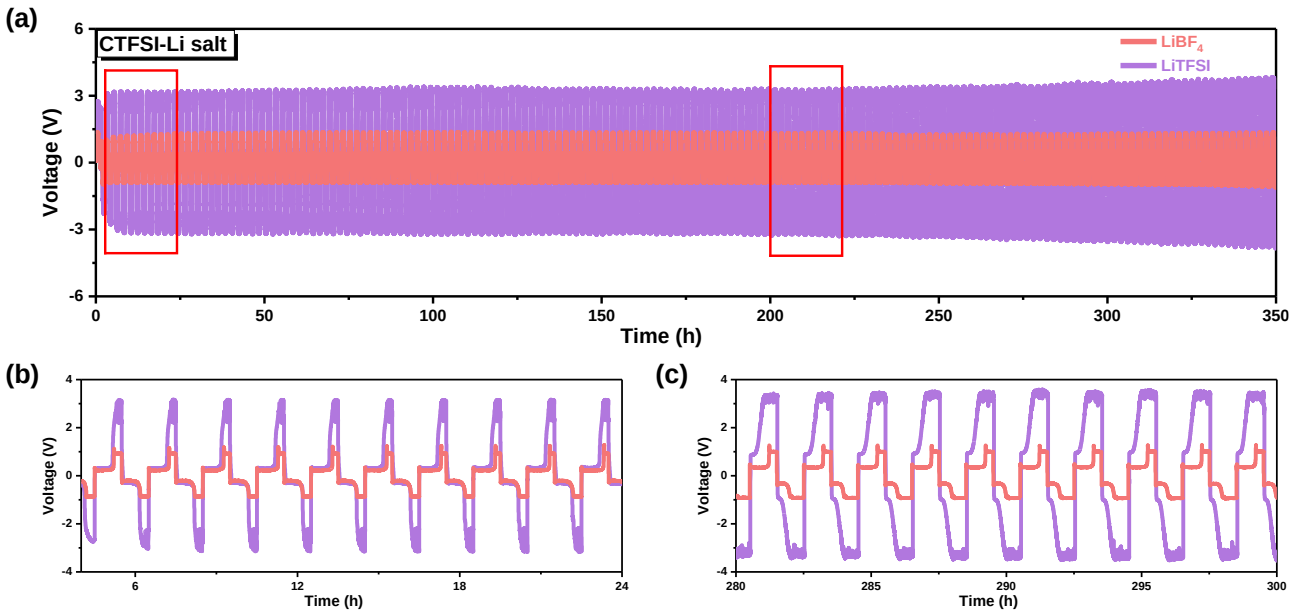

Fig. S34 Time-voltage curves of Ca symmetric cells cycled in various electrolytes with a current density of 0.02 mA cm^{-2} and capacity density of 0.02 mA h cm^{-2}. Voltage-time profiles during (b) 4-24 h and (c) 260-300 h in various electrolytes.

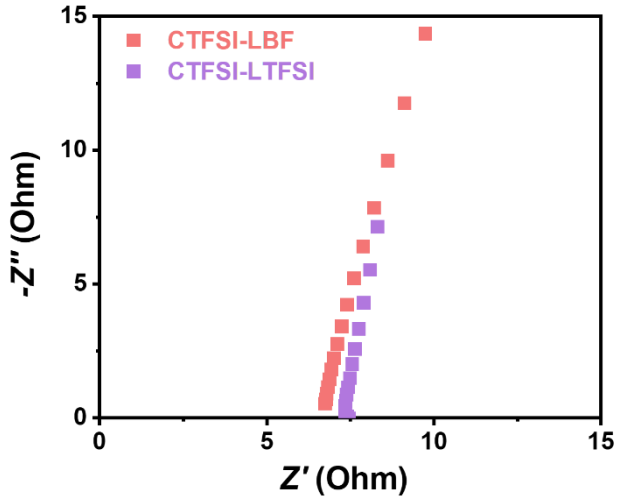

Fig. S35 EIS plots of Ca symmetric cell after various cycles in CTFSI-LBF and CTFSI-LTFSI electrolytes.

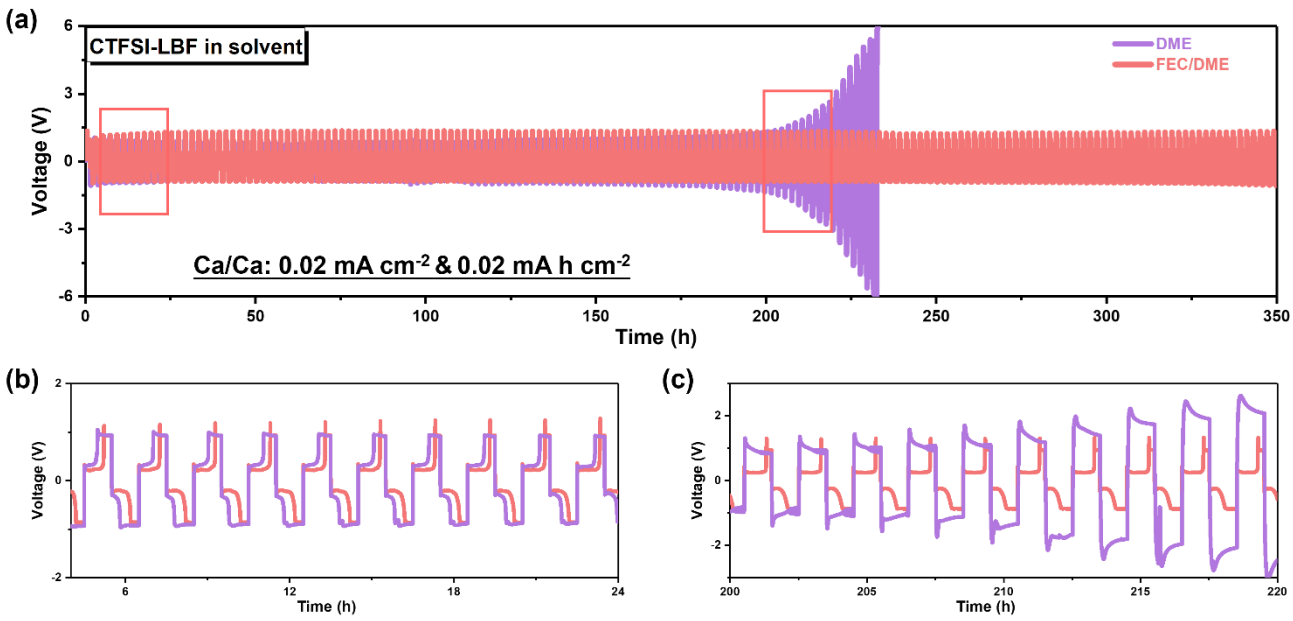

Fig. S36 Time-voltage curves of Ca symmetric cells cycled in various electrolytes with a current density of 0.02 mA cm^{-2} and capacity density of 0.02 mA h cm^{-2}. Voltage-time profiles during (b) 4-24 h and (c) 260-300 h in various electrolytes.

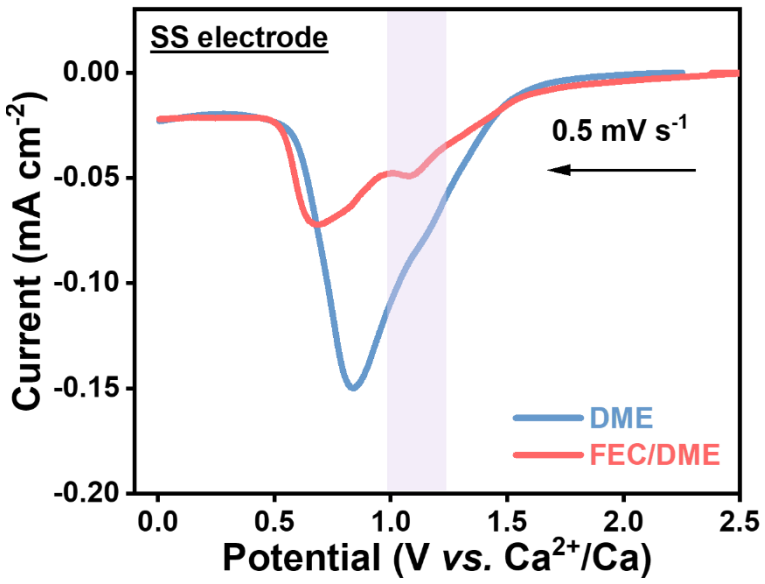

Fig. S37 LSV of SS electrode in CTFSI-LBF dissolve in various solvents in Ca//SS cells from OCP to 0.005 V at a scan rate of 0.5 mV s^{-1}.

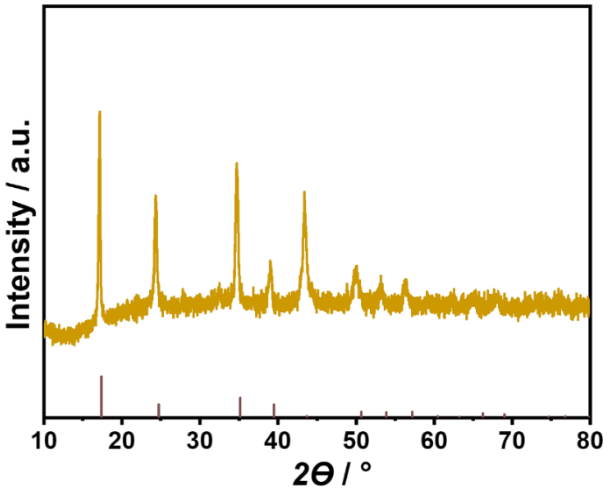

Fig. S38 XRD patterns of Prussian blue analogues cathode.

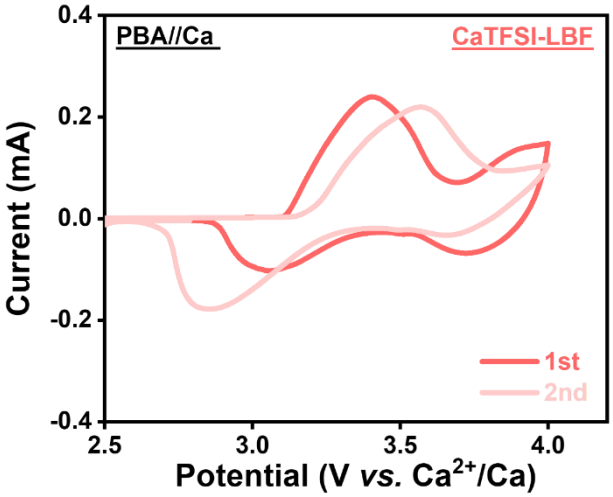

Fig. S39 CV curves of PBA//Ca full cell in CTFSI-LBF electrolyte with a scan rate of 0.1 mV s^{-1} within the voltage range of 2.5-4.0 V.

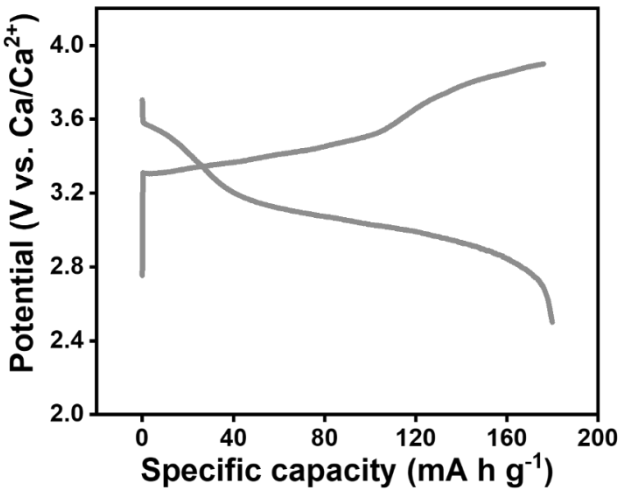

Fig. S40 Charge/discharge curves in PBA//Ca full cell in CTFSI-LBF electrolyte within the voltage range of 2.5-4.0 V.

Table S1 Contents of various elements on SEI derived from baseline and CTFSI-LBF electrolytes.

	N	S	F	O	Other
Baseline	10%	9%	22%	40%	19%
CTFSI-LBF	8%	12%	36%	17%	27%

References

1 W. L. Jorgensen, D. S. Maxwell and J. Tirado-Rives, *J Am Chem Soc*, 1996, 11225–11236.

2 L. S. Dodda, I. C. De Vaca, J. Tirado-Rives and W. L. Jorgensen, *Nucleic Acids Res*, 2017, **45**, W331–W336.

3 J. Wang, W. Wang, P. A. Kollman and D. A. Case, *J Mol Graph Model*, 2006, **25**, 247–260.